Single-neutron energies outside ^{136}Xe

B. P. Kay,[1,*] J. P. Schiffer,[1] S. J. Freeman,[2] C. R. Hoffman,[1] B. B. Back,[1] S. I. Baker,[1] S. Bedoor,[3] T. Bloxham,[4] J. A. Clark,[1] C. M. Deibel,[1,5] A. M. Howard,[2] J. C. Lighthall,[1,3] S. T. Marley,[1,3] K. E. Rehm,[1] D. K. Sharp,[2] D. V. Shetty,[3] J. S. Thomas,[2] and A. H. Wuosmaa[3]

[1]*Physics Division, Argonne National Laboratory, Argonne, Illinois 60439, USA*
[2]*School of Physics and Astronomy, University of Manchester, Manchester M13 9PL, United Kingdom*
[3]*Physics Department, Western Michigan University, Kalamazoo, Michigan 49008, USA*
[4]*Lawrence Berkeley National Laboratory, Berkeley, California 94720, USA*
[5]*Joint Institute for Nuclear Astrophysics, Michigan State University, East Lansing, Michigan 48824, USA*

(Received 4 July 2011; published 29 August 2011)

The single-neutron properties of the $N = 83$ nucleus ^{137}Xe have been studied using the ^{136}Xe(d,p) reaction in inverse kinematics at a beam energy of 10 MeV/u. The helical-orbit spectrometer, HELIOS, at Argonne National Laboratory was used to analyze the outgoing protons, achieving an excitation-energy resolution of ∼100 keV. Extraction of absolute cross sections, angular distributions, and spectroscopic factors has led to a more complete understanding of the single-neutron strength in ^{137}Xe. In particular, the centroids of the $\nu h_{9/2}$ and $\nu i_{13/2}$ strengths appear to evolve through the $N = 83$ isotones in a manner consistent with the action of the tensor force.

DOI: 10.1103/PhysRevC.84.024325 PACS number(s): 25.45.Hi, 21.60.Cs, 27.60.+j

I. INTRODUCTION

Establishing single-particle excitations in nuclei is essential to the framework of our understanding of nuclear structure, and single-nucleon transfer reactions provide an ideal experimental tool for establishing this property. The recent expansion of our experimental knowledge to short-lived nuclei indicates considerable changes in shell structure far from stability (for example, Refs. [1–3]) and has spurred a more detailed investigation of the energies of single-particle excitations in stable nuclei, particularly those where trends can be tracked across a large range of neutron excess such as the Sn isotopes and the $N = 82$ nuclei [4,5].

The motivation for the present measurement was two-fold. One was to extend a previous study of the high-j neutron single-particle states outside the $N = 82$ closed shell [5] by performing the (d,p) reaction on ^{136}Xe in inverse kinematics, thus avoiding the complications of a gaseous Xe target. At the same time, this measurement, with a heavy stable beam, provided a stringent test of the capabilities of the recently commissioned HELIOS spectrometer [6] at the Argonne Tandem-Linac Accelerator System (ATLAS) as the beam used is an order of magnitude heavier than those in the first experiments [7,8].

Recent theoretical investigations [9–11] have been successful in describing the changes in single-particle energies as arising from the tensor component of the nucleon-nucleon interaction. As specific orbits are filling, this interaction causes shifts that depend on whether nucleons are in $j = \ell + 1/2$ or $\ell - 1/2$ orbits and thus modifies the relative proton single-particle energies as the neutron occupancies change or for neutrons as the proton orbits are filled. While the most dramatic consequences of these shifts are in exotic nuclei, the effects can be explored in considerably more quantitative detail in stable nuclei, where more intense beams are available and precision measurements can be performed. Examples of such measurements are in the $Z = 51$ nuclei, where the changes in the $\pi g_{7/2}$ and $\pi h_{11/2}$ states were studied via the (α,t) reaction [4]. Similar measurements, using the $(\alpha,^3\mathrm{He})$ reaction, were performed on the stable $N = 82$ isotones to study the $\nu h_{9/2}$ and $\nu i_{13/2}$ excitations [5]. Such quantitative measurements are becoming possible with unstable nuclear beams [12] and the HELIOS spectrometer was specifically designed for studying reactions performed in inverse kinematics [13].

The focus of the present measurement is to determine the energy centroids corresponding to the nodeless $\nu h_{9/2}$ and $\nu i_{13/2}$ orbitals. These have been studied in the other stable $N = 82$ isotones ($56 \leqslant Z \leqslant 62$) via the (d,p) [14] and $(\alpha,^3\mathrm{He})$ [5] reactions, the latter better matched for $\ell = 5$ and 6 transfer than the (d,p) reaction. Significant fragmentation of the $h_{9/2}$ and $i_{13/2}$ strengths was seen due to mixing of the single-particle excitations with weak-coupling states of the same quantum numbers. From $56 \leqslant Z \leqslant 62$, the difference in the centroids of single-particle strength for the $h_{9/2}$ and $i_{13/2}$ orbitals was found to increase from ∼0.1 to ∼0.5 MeV, in agreement with theoretical calculations incorporating the tensor force [5,16]. Only one $9/2^-$ state had been reported previously for ^{137}Xe, along with an unpublished observation of the lowest $13/2^+$ level [15].

The (d,p) reaction on ^{136}Xe has been studied previously. There are two experiments in the literature done in normal kinematics where a deuteron beam is used to bombard an enriched Xe gas cell [17,18], achieving resolutions of 45 and 80 keV, respectively. A third measurement [19], which constituted the first exploration of direct nucleon transfer in inverse kinematics, achieved an energy resolution of 125–172 keV. These measurements all extracted information for low-ℓ transfer only.

*Present address: Department of Physics, University of York, Heslington, York YO10 5DD, United Kingdom; benjamin.kay@york.ac.uk

II. EXPERIMENT

The measurement was performed at the ATLAS facility at Argonne National Laboratory. A beam of ^{136}Xe was delivered at 10 MeV/u in bunches ∼2 ns wide (FWHM) every 82.47 ns, derived from the intrinsic radio frequency (RF) of the accelerator. At this beam energy, cross sections for transfer to high-ℓ states are larger by a factor of ∼2 compared with yields at ∼6 MeV/u, the energy used in the previous (d,p) studies [17–19]. Typical beam intensities in this measurement were $\sim 5\times10^6$ ions per second; the current was limited to extend the useful life of the deuterated polyethylene $[(C_2D_4)_n]$ targets. Several such targets were used with thicknesses ranging between 125 and 175 μg/cm^2. Outgoing protons, emitted at forward center-of-mass (c.m.) angles ($\theta_{\rm lab} > 90^\circ$) were analyzed in HELIOS, at a field strength of 2 T. Their energy, distance Δz from the target, and time of flight were recorded by an array of position-sensitive Si detectors (PSDs) surrounding the magnetic axis, which corresponds to the beam axis (see Ref. [6]). A schematic of the experimental setup for this measurement is given in Fig. 1.

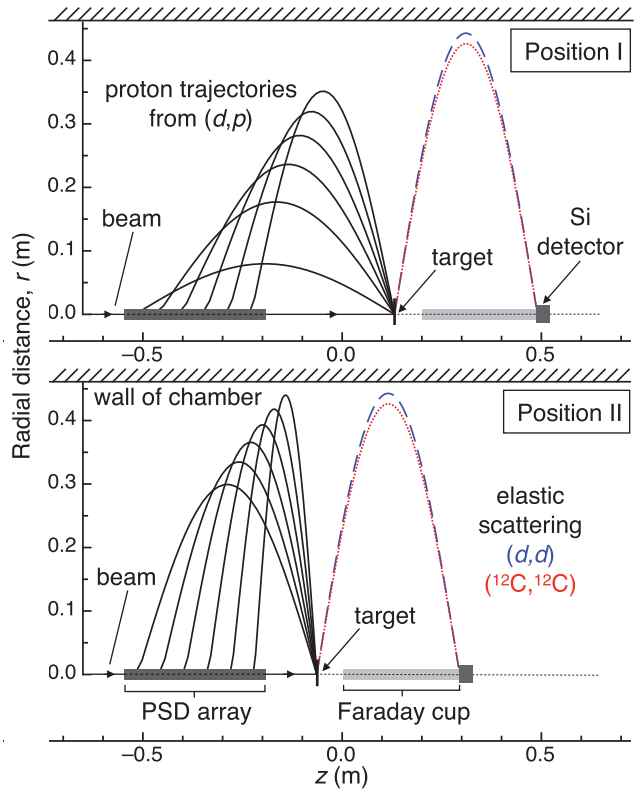

FIG. 1. (Color online) Schematic of the detector and target arrangements in HELIOS. Positions I and II are discussed in the text. The beam enters, on axis, from the left. The radial distance, r, and longitudinal coordinate, z, are given for sample proton trajectories (solid lines). Trajectories of elastically scattered ions, used for monitoring luminosity, are shown by dashed lines for deuterons (blue online), and dotted lines for ^{12}C ions (red online). The z axis is both the beam axis and the magnetic axis where $z = 0.0$ m is the center of the solenoid.

In this measurement, absolute cross sections for the (d,p) reaction are measured to allow for a quantitative comparison with other well-studied $N = 82$ isotones [14]. This was achieved by measuring the luminosity—the product of the beam intensity and the areal density of deuterons in the target—in the arrangement of Fig. 1. The total beam dose was determined from the integrated charge collected in the Faraday cup on the z axis, while elastically scattered deuterons were counted by a Si surface-barrier detector centered on, and with its surface perpendicular to, the z axis. At this z, elastically scattered deuterons intercept the surface of the detector at $\theta_{\rm c.m.} = 34.9^\circ$. To determine the absolute cross-section scale, elastic scattering in the Rutherford regime was measured with the beam energy lowered to 5 MeV/u, where the elastic cross section at this laboratory angle ($\theta_{\rm c.m.} = 29.2^\circ$) is within ±3% of the Rutherford scattering cross section.

From previous studies with standard polyethylene targets, it is known that these can degrade under beam irradiation [20]. Elastically scattered carbon ions (charge state $q = 6^+$) are also detected in the luminosity monitor but with approximately six times the energy. This allowed a continuous monitoring of both the target thickness and composition. Typically, the targets would lose carbon and deuterium at similar rates, reaching 50% of the original number of atoms after a dose of $\sim 5\times10^{11}$ ^{136}Xe ions with a beam spot of ∼3-mm diameter.

Data were collected over 59 hours of beam on target. Of the 24 PSDs on the array, 18 were functional for this experiment. A composite plot of data from the PSD array is presented in Fig. 2. Two target positions were used to cover the largest possible c.m.-angle range; for $\ell = 5$ and 6 transfer, the peak cross sections were expected to be at $\theta_{\rm c.m.} \sim 32^\circ$ and 40°, respectively. The positions of the target are shown schematically in Fig. 1; data from the two positions are labeled in the upper portion of Fig. 2. For each PSD, the slope in energy versus position was corrected using a fourth-order polynomial to account for nonlinear responses. The internal excitation-energy calibration was performed on a detector-by-detector basis, using well-known states in ^{137}Xe. This procedure was cross checked with an absolute energy calibration using a multiline α source (^{148}Gd-^{244}Cm) performed before and after the experiment. The α source also served as a check of the detector-to-detector efficiency. In principle, the α source should irradiate each PSD with the same number of α particles as each PSD subtends the same solid angle and the α particles are emitted isotropically. Due to varying PSD performance and possible small misalignments of either the PSD array or the target assembly, this is not the case. Data from the α source provided a normalization to correct for these variations.

Events corresponding to one proton cyclotron period could be clearly identified; these correspond to a time difference of 32.8 ns between the accelerator RF and a proton intercepting the array (the timing resolution was ∼8 ns FWHM). Peaks were also seen at 65.6 and 98.4 ns, corresponding to protons that had performed two and three cyclotron periods before intercepting the array, respectively, and these were readily eliminated. Protons from fusion evaporation of the xenon beam with carbon in the target were indistinguishable from the protons of interest and account for the overall background seen in the upper part of Fig. 2. This background contribution

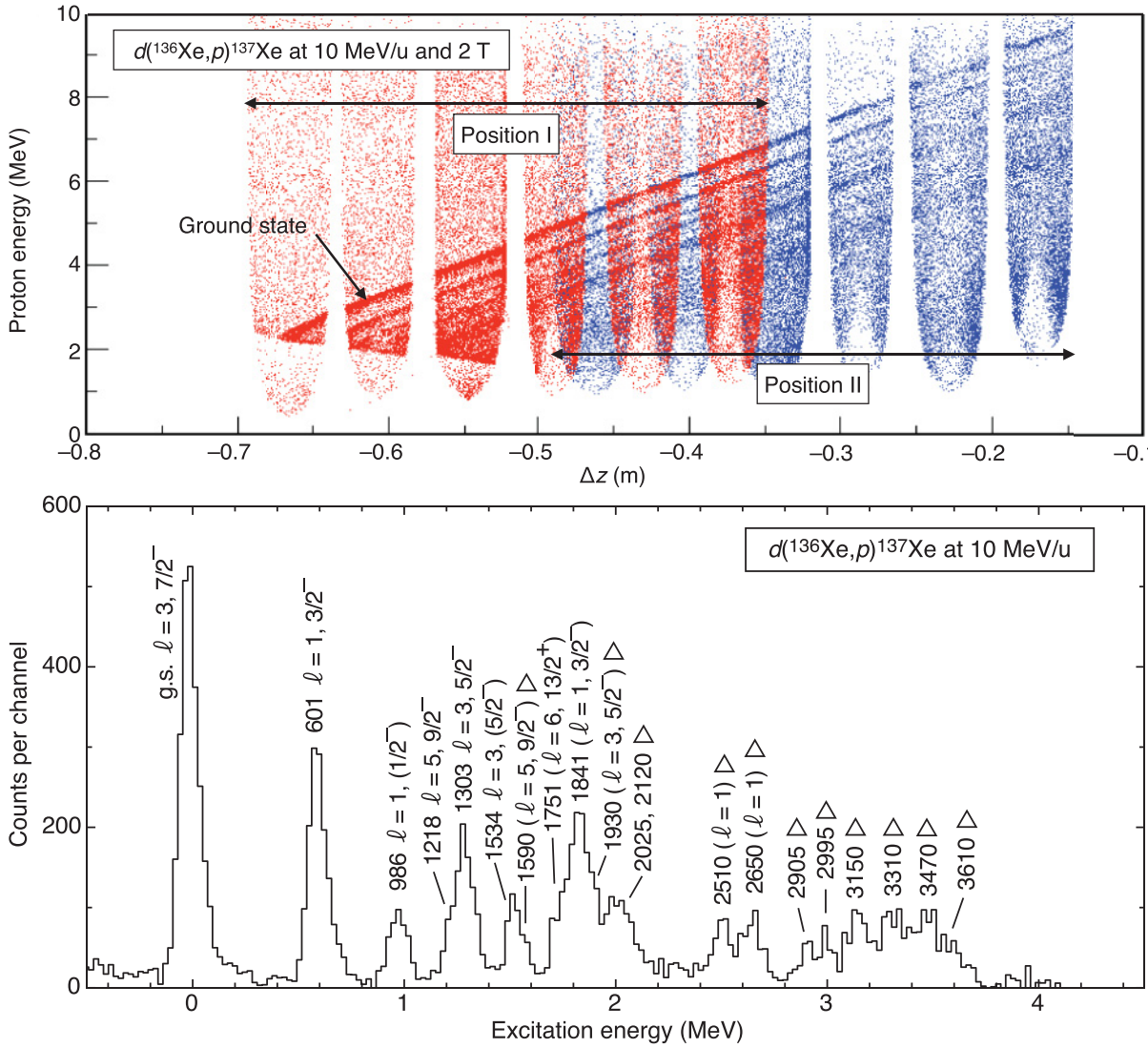

FIG. 2. (Color online) (Top) Proton energy versus longitudinal distance traveled between the target and the point of impact on the Si array, Δz, for the $d(^{136}\mathrm{Xe},p)^{137}\mathrm{Xe}$ reaction at 10 MeV/u and a 2-T field. The plot is a composite of two different target positions, as discussed in the text. (Bottom) Representative proton spectrum. Peaks are labeled by their energy (to the nearest keV) and by their ℓ value, spin, and parity, where these quantities are known. States marked with a △ symbol are those with energy, ℓ value, or both, deduced for the first time in this work. A smooth background has been subtracted to produce the displayed spectrum as discussed in the text.

was smooth and was subtracted in the analysis, the associated uncertainty in the extracted yields is discussed below.

The proton data were binned according to their position z along the beam axis. A typical spectrum of proton energy versus Δz, the distance between the target and point of impact on the array, is given in the upper portion of Fig. 2. The sloping lines in this plot correspond to the population of different excited states in the final nucleus; the ground state is labeled for illustration. The locus of a line for a particular final state corresponds to different proton angles. The central position of each PSD on the array, at the two target-array distances, was chosen as the set of angles for the angular distributions, although the corresponding c.m. angle does depend on the excitation energy. For the angular distributions, the data were binned according to the angular range covered by the respective PSDs; however, in HELIOS, each PSD subtends equal solid angle in the c.m. frame. The yields to specific final states were extracted for each of these angles and normalized, using the elastic-scattering data, to produce absolute cross sections.

Several factors that contribute to the cross-section uncertainties are estimated here. The solid angle of the monitor detector is the dominant source of systematic uncertainty and is estimated to be ∼11%. With typical beam intensities of $\sim 5 \times 10^6$ ions per second, the beam current integrator was near the limit of its sensitivity, and the corresponding uncertainty is estimated to be 5%. From α-source data, the yield due to the performance of individual PSDs was found to have an rms variation of ∼7%. The uncertainty in the measurement of the Rutherford scattering cross section is at the

∼3% level. A smooth background, generated by protons from fusion-evaporation of the target and the beam, was subtracted prior to fitting peaks. To first order, this was linear in the range of 0–3.7 MeV in excitation energy. This subtraction is considered to contribute <5% uncertainty to the cross sections. The combined uncertainty in the absolute cross sections is, thus, estimated to be on the order of 15%.

A typical excitation-energy resolution of ∼100 keV was achieved, though there was variation across the PSD array based on the properties of the individual detectors. The range of this variation was 90 to 130 keV and independent of position in z. The observed resolution is a consequence of several factors; the dominant sources are the intrinsic detector resolution ($\gtrsim$50 keV and varied from 50–90 keV among the detectors [6]), the beam energy loss in the target, and the proton energy loss and straggling in the target. The beam energy loss in the target is ∼10 MeV for these targets and contributes ∼10–40 keV to the resolution for $\theta_{\mathrm{c.m.}} \sim 5$–$30^{\circ}$, respectively. The proton energy losses are similar across the angular range of interest; the higher stopping power of the lower energy protons is offset by traversing less target thickness, since they travel on trajectories closer to the solenoid axis. Protons with higher energy are emitted at less backward laboratory angles that see a greater geometric target thickness but have a lower stopping power. This is estimated to contribute ∼20 keV to the resolution. For this experiment, the beam energy spread was <2%, with a diameter of $\lesssim$3 mm, as determined by the aperture on the tuning cup. The size of the beam spot contributes $\lesssim$ 20 keV to the energy resolution in Fig. 2. From the outgoing proton spectra, the change in resolution over the excitation-energy range where discrete peaks could be fitted is negligible.

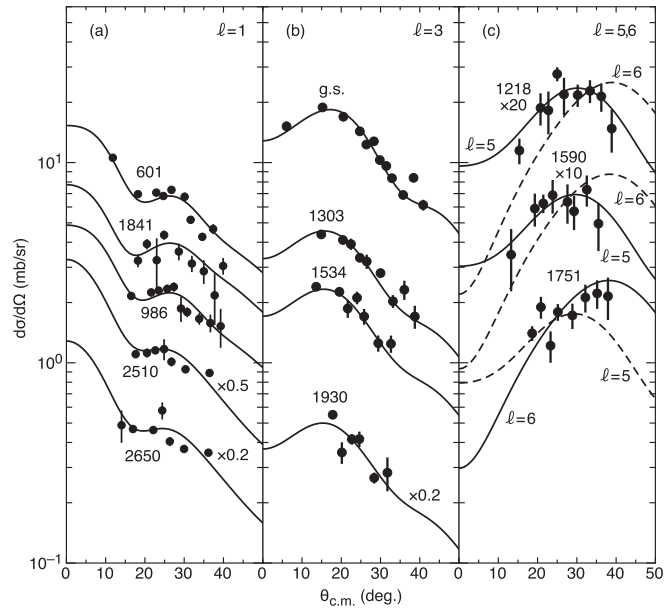

FIG. 3. Angular distributions for the outgoing protons in the $d(^{136}\mathrm{Xe},p)^{137}\mathrm{Xe}$ reaction. Panels (a), (b), and (c) group the $\ell = 1$, 3, 5 and 6 angular distributions, respectively. Some data have been scaled by a multiplicative factor, labeled on the plots. The solid circles represent the data—the error bars convey the statistical uncertainty—while the curves are DWBA calculations normalized to fit the data. States are labeled by their energy in keV and their assigned ℓ value. For the high-ℓ transfer, where the angular distributions for $\ell = 5$ and 6 are similar, both fits are shown; the best fit as a solid line, the other as a dashed line.

III. RESULTS AND DISCUSSION

A representative ^{137}Xe excitation-energy spectrum for $-0.488 \leqslant \Delta z \leqslant -0.437$ m is presented in the lower portion of Fig. 2. Eight previously known states [15,21] are seen clearly. Angular distributions (see Fig. 3) were extracted where feasible, with the remaining states being either too weak or not resolved. DWBA calculations were carried out using the finite-range code Ptolemy [23] with several sets of optical-model parameters [24]. Those used to deduce the spectroscopic factors of Table I and subsequent analysis are from Ref. [14]. For the deuteron bound-state wave function, a Reid potential [25] was used. The final neutron bound state was modeled using a Woods-Saxon potential of radius $r_0 = 1.25$ fm and diffuseness $a_0 = 0.63$ fm, whose depth was adjusted to reproduce the experimental binding energy. Absolute spectroscopic factors are highly sensitive to the final bound state radius with a 5% increase resulting in a ∼40% change magnitude. However, the relative spectroscopic factors, between states of different energy and ℓ values, vary by less than 15%. A variation of approximately 25% was seen in the absolute spectroscopic factors between the different optical-model parameter sets; the variation in the relative spectroscopic factors was approximately 10%.

Angular distributions for the states at 0, 601, 986, 1218, 1303, 1534, and 1841 keV are in agreement with previously assigned ℓ values [21]. Based on the systematics of particle-vibration coupling in the $N = 83$ isotones, two states are expected to carry the $\nu h_{9/2}$ strength, as shown in Fig. 4(a). The first $9/2^-$ level is seen at 1218 keV; the second one was previously unknown. The state at 1590 keV, which forms a doublet with the 1534-keV level, is found to have an angular distribution consistent with $\ell = 5$ transfer. Here, it is assigned as the missing $9/2^-$ state. An assignment of $13/2^+$ is made to the state at 1751 keV, in line with a previously unpublished assignment [15]. The peaks at 1590, 1930, 2510, and 2650 keV could correspond to states at these energies and have not been previously reported. Their angular distributions suggest $\ell = 5$, 3, 1, and 1, respectively. No reliable angular distributions could be extracted for the peaks at 2025, 2120, 2905, 2995, 3150, 3310, 3470, and 3610 keV. In the literature, there are states close in energy to those reported here, but they cannot be definitively associated with the observed peaks.

The measured energies, cross sections, and spectroscopic factors (where deduced) for final states populated in the present measurement are listed in Table I. The trends of the $9/2^-$ and $13/2^+$ states, and the reconstructed $\nu h_{9/2}$ and $\nu i_{13/2}$ centroids, are provided in Fig. 4. The fragmentation of the $\nu h_{9/2}$ and $\nu i_{13/2}$ strength is attributed to two-state mixing between core-coupled configurations: $0^+_{\mathrm{core}} \otimes \nu i_{13/2}$ and $3^-_{\mathrm{core}} \otimes \nu f_{7/2}$, in the case of the $13/2^+$ states, and $0^+_{\mathrm{core}} \otimes \nu h_{9/2}$ and $2^+_{\mathrm{core}} \otimes \nu f_{7/2}$, in

TABLE I. Energies, ℓ values, spins and parities, and spectroscopic factors for states in ^{137}Xe as populated in the (d,p) reaction on ^{136}Xe at 10 MeV/u. The spectroscopic factors are cross-section-weighted averages over the angle range measured; the cross sections quoted are at, or near, the maxima—the specific angles, to the nearest degree, are shown in parentheses. The uncertainties in cross sections and relative spectroscopic factors are discussed in the text. Energies of states determined in this work have an estimated uncertainty of 20 keV. ℓ values and spins and parities given in parentheses are tentative.

E (keV)	ℓ ($\hbar$)	J^π	$\sigma(\theta)$ (mb/sr)	C^2S
0.0[a]	3	$7/2^-$	18.8 (15°)	0.94
601[a]	1	$3/2^-$	10.6 (12°)	0.52
986[a]	1	$1/2^-$,$3/2^-$	2.2 (17°)	0.35
1218[a]	5	$9/2^-$	1.1 (33°)	0.43
1303[a]	3	$5/2^-$	4.4 (15°)	0.22
1534[a]	3	$5/2^-$,$7/2^-$	2.2 (20°)	0.12
1590	(5)	$(9/2^-)$	0.7 (33°)	0.24
1751[b]	(6)	$(13/2^+)$	1.8 (38°)	0.84
1841[a]	(1)	$(1/2^-,3/2^-)$	3.9 (25°)	0.29
1930	(3)	$(5/2^-,7/2^-)$	2.8 (18°)	0.10
2025	(1,3)	–	2.1 (20°)	0.22/0.15
2120	(1,3)	–	0.9 (19°)	0.09/0.06
2510	(1)	$(1/2,3/2^-)$	2.0 (23°)	0.19
2650	(1)	$(1/2,3/2^-)$	2.1 (22°)	0.16
(2905)[c]	(1,3)	–	0.8 (16°)	0.08/0.05
(2995)[c]	(1,3)	–	1.4 (21°)	0.16/0.05
(3150)[c]	–	–	0.3 (35°)	–
(3310)[c]	–	–	0.3 (35°)	–
(3470)[c]	–	–	0.5 (34°)	–
(3610)[c]	–	–	0.4 (34°)	–

[a]States known from previous work [21] and used for calibrating the excitation energy.
[b]Energy and spin assignment previously reported in Ref. [15].
[c]Peaks are observed at these energies, though it cannot be ruled out that these are multiplets.

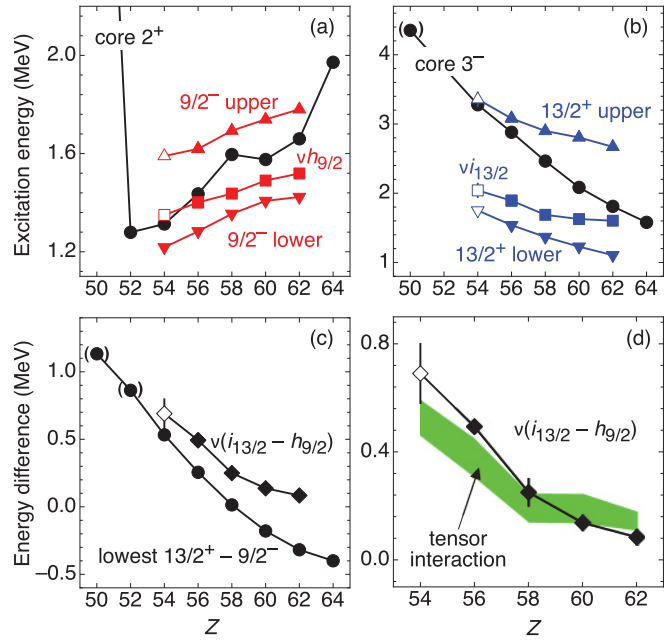

FIG. 4. (Color online) Extension of the plots found in Ref. [5]. (a) The energies of the $9/2^-$ states and the centroids of the $\nu h_{9/2}$ strength for the $N = 83$ isotones plotted against the core 2^+ energies; (b) the energies of the $13/2^+$ levels and the centroids of the $\nu i_{13/2}$ strength against the core 3^- energies. The energy differences between the lowest $13/2^+$ and $9/2^-$ states (circles) and in the $\nu i_{13/2}$ and $\nu h_{9/2}$ centroids (diamonds) are given in (c); in (d) the energy difference in the centroids is compared to the tensor interaction calculations [16]. In all four plots, the solid symbols are data from the literature [5,21,22] and the open symbols are from this work. Data for the unobserved upper $13/2^+$ state have been estimated using the method outlined in the text.

the case of the $9/2^-$ levels. On the basis of this simple model, mixing matrix elements were calculated for $56 \leqslant Z \leqslant 62$ and were found to be remarkably constant; their values can be found in Ref. [5].

The observation of both $9/2^-$ states in this work corresponds to a smooth continuation of the trends, both in the energy systematics of individual states and the centroid of single-particle strength, which is extracted from the spectroscopic-factor weighted energies of the fragments. The lower $9/2^-$ state runs closer to the core 2^+ as Z decreases, which is reflected in the percentage of strength in the upper $9/2^-$ state: 36(5)% at ^{137}Xe (this work), 37(2)% at ^{139}Ba, 27(3)% at ^{141}Ce, 26(1)% at ^{143}Nd, and 29(3)% at ^{145}Sm [5].

For the $13/2^+$ states, only the lowest-lying level was observed in this measurement. An estimate of the strength and location of the upper $13/2^+$ state was made, based on the work of Ref. [5]. Taking the mixing matrix-element value and assuming a spectroscopic strength for the second $13/2^+$ state (based on comparisons with the percentage of strength in the upper fragment of the heavier $N = 83$ isotones), its energy, and therefore the centroid of single-particle strength, can be deduced given the known energy of the core 3^- state. It is estimated to lie at 3360(110) keV with a spectroscopic factor of 0.15(4). From Table I, it can be seen that this is close to the peaks observed at 3310 and 3470 keV. The estimated spectroscopic factor is consistent with both of these, 0.11 and 0.17, respectively, if a $13/2^+$ assignment is assumed. The uncertainty in both the energy and the spectroscopic factor is set by the extremes of the 3310- and 3470-keV peaks. It cannot be ruled out, however, that these experimental peaks contain other strengths—the statistics at these excitation energies were insufficient to determine properly that the observed experimental peaks are not multiplets of transitions to several states. Based on these calculations using data from previous work and a plausible comparison to the tentatively observed peaks, the energy and spectroscopic factor quoted above are used for the $13/2^+$ state in Figs. 4(b), 4(c) and 4(d). The large uncertainty is reflected in the error bar for the difference in the centroids for the $\nu h_{9/2}$ and $\nu i_{13/2}$ strength seen in Figs. 4(c) and 4(d).

Calculations with the tensor interaction [9,16] result in a reduction in the separation of the $\nu h_{9/2}$ and $\nu i_{13/2}$ orbitals by 0.18 MeV per additional proton occupying the $\pi g_{7/2}$ orbital. The large overlap in the radial wave function of these nodeless orbitals makes this the dominant contribution to the reduction in separation of $\nu h_{9/2}$ and $\nu i_{13/2}$ orbitals: a weaker contribution

is induced by the $\pi d_{5/2}$ protons, which fill the cores at a similar rate to the $\pi g_{7/2}$ protons (from $54 \leqslant Z \leqslant 62$). This results in an increase in the separation of the $\nu h_{9/2}$ and $\nu i_{13/2}$ orbitals by 0.04 MeV per additional proton: far weaker due to the poor overlap between the respective radial wave functions. As in Ref. [5], the adopted proton occupancies were those deduced in the work of Wildenthal *et al.* [26]; the spread in the theory is due to the experimental uncertainty in the occupancies. The calculations based on the tensor force are shown in Fig. 4(d) and are consistent with the experimental data for the single-neutron energies outside the stable $N = 82$ isotones.

In conclusion, the neutron-adding (d,p) on ^{136}Xe reaction has been performed in inverse kinematics at a beam energy of 10 MeV/u populating single-particle states in ^{137}Xe. Outgoing protons were analyzed by the HELIOS spectrometer with an excitation-energy resolution of 90–130 keV. Cross sections, angular distributions, and spectroscopic factors have been extracted from the data where possible. This is the first use of the HELIOS spectrometer with heavy beams. It clearly demonstrates its potential for future studies with radioactive ion beams around the $Z = 50$ and $N = 82$ shell closures. The centroids of the $\nu h_{9/2}$ has been determined and that of the $\nu i_{13/2}$ strength inferred; the evolution of these states through the $N = 83$ nuclei behaves in a manner consistent with the action of the tensor force.

ACKNOWLEDGMENTS

The authors would like to thank the ATLAS operations crew, J. P. Greene for the preparation of targets, and T. Otsuka for providing the matrix elements used. This work was supported by the US Department of Energy, Office of Nuclear Physics, under Contract No. DE-AC02-06CH11357 and Grant No. DE-FG02-04ER41320, and NSF Grant No. PHY-08022648 (JINA), and the UK Science and Technology Facilities Council.

[1] A. Ozawa, T. Kobayashi, T. Suzuki, K. Yoshida, and I. Tanihata, Phys. Rev. Lett. **84**, 5493 (2000).
[2] C. R. Hoffman *et al.*, Phys. Lett. B **672**, 17 (2009).
[3] R. Kanungo *et al.*, Phys. Rev. Lett. **102**, 152501 (2009).
[4] J. P. Schiffer *et al.*, Phys. Rev. Lett. **92**, 162501 (2004).
[5] B. P. Kay, S. J. Freeman, J. P. Schiffer, J. A. Clark, C. Deibel, A. Heinz, A. Parikh, and C. Wrede, Phys. Lett. B **658**, 216 (2008).
[6] J. C. Lighthall *et al.*, Nucl. Instrum. Methods Phys. Res. A **622**, 97 (2010).
[7] B. B. Back *et al.*, Phys. Rev. Lett. **104**, 132501 (2010).
[8] A. H. Wuosmaa *et al.*, Phys. Rev. Lett. **105**, 132501 (2010).
[9] T. Otsuka, T. Suzuki, R. Fujimoto, H. Grawe, and Y. Akaishi, Phys. Rev. Lett. **95**, 232502 (2005).
[10] T. Otsuka, T. Suzuki, M. Honma, Y. Utsuno, N. Tsunoda, K. Tsukiyama, and M. Hjorth-Jensen, Phys. Rev. Lett. **104**, 012501 (2010).
[11] N. A. Smirnova, B. Bally, K. Heyde, F. Nowacki, and K. Sieja, Phys. Lett. B **686**, 109 (2010).
[12] K. Jones *et al.*, Nature (London) **465**, 454 (2010).
[13] A. H. Wuosmaa, J. P. Schiffer, B. B. Back, C. J. Lister, and K. E. Rehm, Nucl. Instrum. Methods Phys. Res. A **580**, 1290 (2007).
[14] W. Booth, S. Wilson, and S. S. Ipson, Nucl. Phys. A **229**, 61 (1974).
[15] D. C. Radford (private communication).
[16] T. Otsuka (private communication).
[17] E. J. Schneid and B. Rosner, Phys. Rev. **148**, 1241 (1966).
[18] P. A. Moore, P. J. Riley, C. M. Jones, M. D. Mancusi, and J. L. Foster Jr., Phys. Rev. **175**, 1516 (1968).
[19] G. Kraus *et al.*, Z. Phys. A **340**, 339 (1991); G. Kraus, Diploma Universität Mainz (1990); G. Kraus, Gesellschaft für Schwerionenforschung mbH, Report GSI-90-04 (1990).
[20] K. E. Rehm *et al.*, Nucl. Instrum. Methods Phys. Res. A **418**, 355 (1998).
[21] E. Browne and J. K. Tuli, Nucl. Data Sheets **108**, 2173 (2007).
[22] A. A. Sonzogni, Nucl. Data Sheets **95**, 837 (2002).
[23] M. H. Macfarlane and S. C. Pieper, ANL-76-11 Rev. 1, ANL Report (1978).
[24] A total of 11 optical-model-parameter sets were explored, including those presented in Refs. [14,17] and J. C. Veefkind *et al.*, Z. Phys. A **275**, 55 (1975); J. Lien *et al.*, Can. J. Phys. **55**, 463 (1977); A. Strömich *et al.*, Phys. Rev. C **16**, 2193 (1977); I. Tomandl *et al.*, Nucl. Phys. A **717**, 149 (2003).
[25] R. V. Reid, Ann. Phys. **50**, 411 (1968).
[26] B. H. Wildenthal, E. Newman, and R. L. Auble, Phys. Rev. C **3**, 1199 (1971).